

# Linker Exchange via Migration along the Backbone in Metal–Organic Frameworks

Nader Al Danaf, Waldemar Schimpf, Patrick Hirschle, Don C. Lamb, Zhe Ji,\* and Stefan Wuttke\*

 Cite This: *J. Am. Chem. Soc.* 2021, 143, 10541–10546

 Read Online

ACCESS |

 Metrics & More

 Article Recommendations

 Supporting Information

**ABSTRACT:** In metal–organic frameworks (MOFs), organic linkers are subject to postsynthetic exchange (PSE) when new linkers reach sites of PSE by diffusion. Here, we show that during PSE, a bulky organic linker is able to penetrate narrow-window MOF crystals. The bulky linker migrates by continuously replacing the linkers gating the otherwise impassable windows and serially occupying an array of backbone sites, a mechanism we term *through-backbone diffusion*. A necessary consequence of this process is the accumulation of missing-linker defects along the diffusion trajectories. Using fluorescence intensity and lifetime imaging microscopy, we found a gradient of missing-linker defects from the crystal surface to the interior, consistent with the spatial progression of PSE. Our success in incorporating bulky functional groups via PSE extends the scope of MOFs that can be used to host sizable, sophisticated guest species, including large catalysts or biomolecules, which were previously deemed only incorporable into MOFs of very large windows.

Metal–organic frameworks (MOFs) are extended, porous structures built by connecting metal-containing clusters with organic linkers.<sup>1</sup> These rigid, sizable molecular building units create interconnected pore space amenable to guest incorporation and chemical functionalization, by, for instance, using organic linkers bearing chemical moieties of interest.<sup>2,3</sup> To incorporate a functionalized linker, a strategy termed postsynthetic exchange (PSE) has been developed, presynthesized MOFs are soaked in the solution of a new linker, which replaces the original linker without altering the overall MOF structures.<sup>4–13</sup> Applying PSE enables the synthesis of otherwise unattainable MOFs when *de novo* synthesis results in linker decomposition or amorphous products.<sup>14</sup>

When performing PSE, it is a common practice to choose a linker smaller than the window (*i.e.*, pore aperture) of the MOF, for fear that a larger linker will be blocked from accessing the interior of MOF crystals. This is based on the assumption that the new linker has to first diffuse through windows before reaching the site of PSE at a distant pore.<sup>15</sup> We sought to explore the possibility of performing PSE in a prototypical MOF, UiO-67,<sup>16</sup> using a bulky linker, biphenyl-4,4'-dicarboxylic acid attached with rhodamine b (BPDC-RB, Figure 1a), a fluorophore serving to report PSE progression. RB is small enough to fit in the octahedral pore in UiO-67, yet larger than the window (Figure 1b, Figure S5, and section S2 in the Supporting Information), through which diffusion cannot occur (Figure S6). Surprisingly, we observed a substantial amount of BPDC-RB incorporated into the interior of UiO-67 crystals. This is not due to the windows enlarged by missing-linkers (Figure S7); a low fraction of missing-linkers (<0.2%) was found in the UiO-67 crystals that we synthesized (Figure S7). Additionally, UiO-67 is a rather rigid MOF that cannot undergo excessive pore swelling or breathing necessary for accommodating incoming bulky linkers.<sup>17</sup> Hence, there

must be a mechanism different from through-window diffusion (Figure 1c) for PSE.

We postulated that a bulky linker could migrate across a narrow-window MOF by continuously replacing the linkers gating the windows. When an original linker dissociates from the MOF backbone under PSE conditions,<sup>18</sup> it opens the otherwise narrow window,<sup>19</sup> allowing the new linker to move its bulky group from one pore to the other and then reinsert into the backbone (Figure 1d). The net result is that the new linker migrates along the MOF backbone by one pore; multiple rounds of these actions enable diffusion for a long distance within the crystal. We term this process *through-backbone diffusion* to distinguish it from the conventional *through-window diffusion*.

For migration from the crystal surface all the way to the center, through-backbone diffusion requires PSE to occur in every pore that the new linker passes through. Every time the linker transits toward the next pore, it has to first dissociate from the current site of the backbone, leaving behind a vacancy (*i.e.*, missing-linker defect). This eventually results in an array of missing-linker defects along the diffusion trajectory (Figure 1d), provided that the defects are not healed by other free linkers. In contrast, through-window diffusion creates only one defect when the migrating linker departs from the backbone; no more defects are created because it passes through windows without PSE (Figure 1c).

Received: May 9, 2021

Published: July 6, 2021



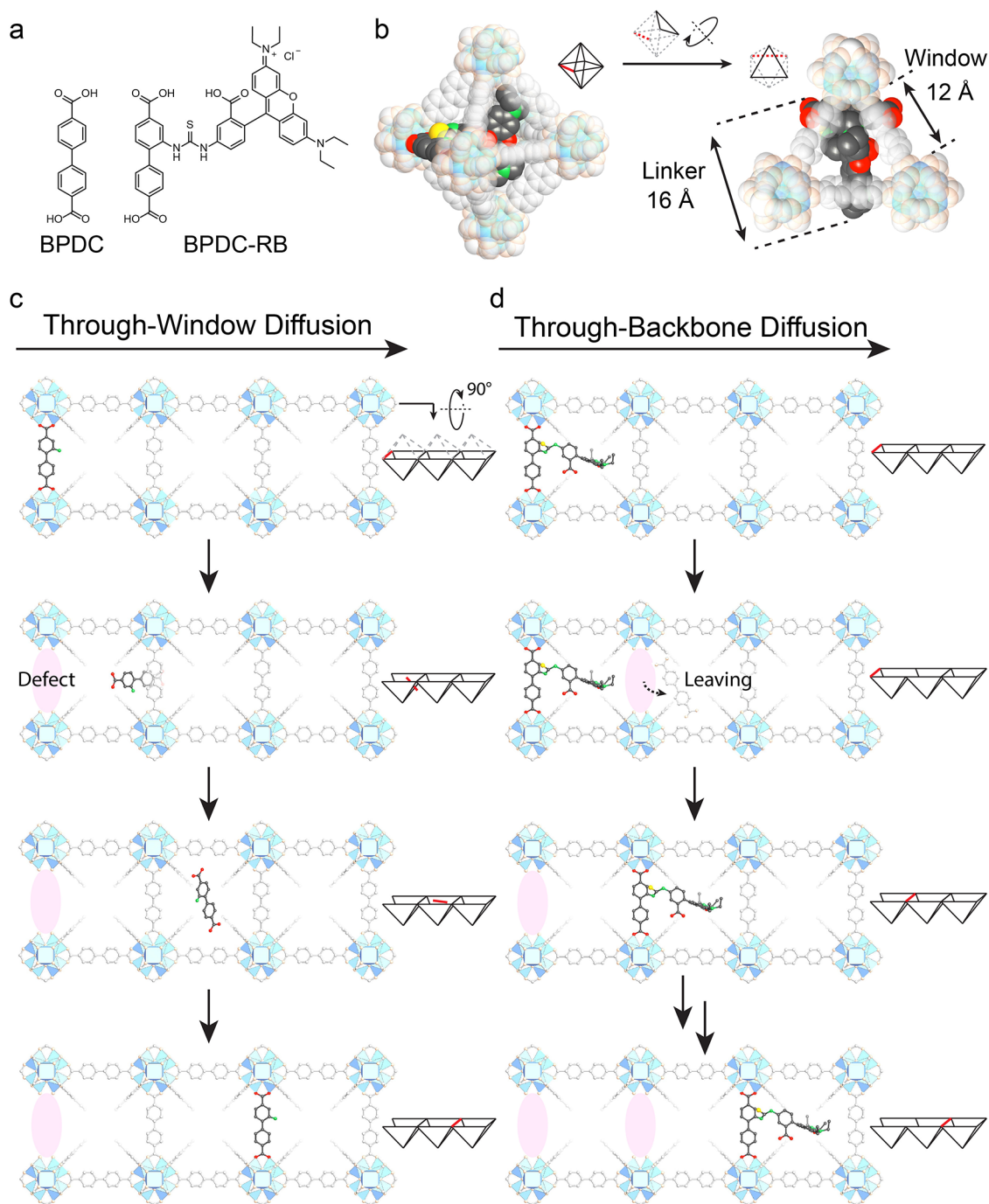


**Figure 1.** (a) Molecular structures of BPDC and BPDC-RB. (b) Space-filling model of an octahedron unit in UiO-67, which comprises a BPDC-RB linker, and a projection of BPDC-RB beneath a triangular window. (c) Structure illustration of through-window diffusion of a small linker and (d) through-backbone diffusion of the bulky linker BPDC-RB in UiO-67. The horizontal arrows indicate the average direction of many diffusion events, which follows the concentration gradient established from the crystal surface to its center. Color code for BPDC-RB: C, gray; O, red; S, yellow; N, green. Color code for other UiO-67 components: Zr cluster, blue; C and O, off-white.

Here, we use fluorescence imaging to monitor the migration of the bulky BPDC-RB linker across UiO-67 crystals and observed that the PSE propagated from the surface to the center of the crystals, establishing a concentration gradient of the new linker. To investigate how the bulky linker can migrate across the narrow-window MOF, we performed fluorescence lifetime imaging microscopy (FLIM)<sup>20</sup> to examine the change in the chemical environment<sup>21–23</sup> along the PSE gradient. The lifetime was observed to decline toward the edge of the crystal, indicating the accumulation of missing-linker defects during

PSE, a distinctive feature supporting the through-backbone diffusion mechanism.

UiO-67 was synthesized as single crystals ( $\sim 50 \mu\text{m}$ ), far larger than the spatial resolution of conventional fluorescence microscopy, therefore serving as a suitable object for our studies. The obtained crystals were subjected to PSE through incubation with BPDC-RB in a mixture of methanol (MeOH) and *N,N'*-dimethylformamide (DMF) at a ratio of 80:20 (v/v). We chose this solvent mixture (MeOH/DMF) because it has been reported that MeOH facilitates linker substitution in

UiO-67<sup>18</sup> and DMF allows for high temperature incubation. To investigate the effect of time and temperature on PSE, incubation was performed at room temperature or 100 °C for 1 day or for 7 days (1d-RT, 1d-100 °C, 7d-RT, and 7d-100 °C). After PSE, we did not observe any change in crystal morphology and crystallinity (Figure S9) or any photophysical damage to the RB moiety (Figures S10–S12 and Table S1).

Fluorescence intensity imaging microscopy was employed to measure the spatial distribution of BPDC-RB incorporated inside UiO-67 crystals. These crystals, octahedral in shape (Figure 2a), were oriented along the [111] direction, with

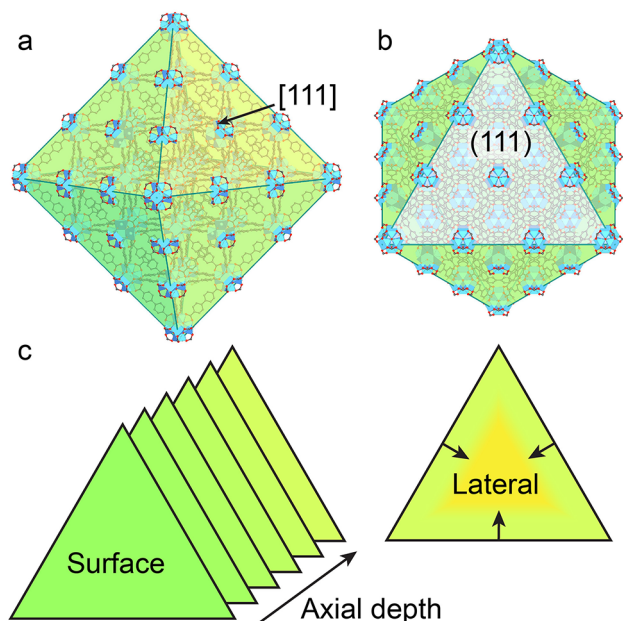


**Figure 2.** (a) Schematic diagram of an octahedral crystal of UiO-67, (b) crystal is oriented along the [111] direction, and (c) fluorescence and lifetime images were collected both laterally and axially.

triangle and hexagonal cross sections displayed on the focal plane (Figure 2b). The fluorescence intensity of RB was mapped in the focal plane (lateral) and along the optical axis (axial) (Figure 2c), both displaying a profile that peaks at the surface and slowly decreases toward the center (Figure 3).

We noticed that progression of PSE is highly dependent on the incubation temperature. A significant increase in fluorescence was observed when performing PSE at 100 °C as compared to RT (Figure 3a–d). At RT, a longer reaction time led to more PSE on the surface but was not effective in promoting PSE in the crystal interior. In contrast, longer reaction times at 100 °C resulted in more BPDC-RB penetrating into the crystals. The solvent dependence of PSE was tested by using DMF as an alternative solvent. For DMF, PSE was found sluggish and required high temperature to achieve any noticeable progress (Figure S14). The heterogeneous distribution of BPDC-RB, which concentrates on the surface and declines toward the crystal interior, reveals that linker diffusion becomes the rate-limiting step of PSE. This step, unlike the free diffusion of linkers in solution and in large-window MOFs, likely involves a high energy barrier, indicated by the dependence of PSE progression on temperature, time (weekly scale), and solvent. In fact, the diffusion of RB alone is prohibited inside UiO-67. After soaking UiO-67 crystals with RB in DMF for 7 days, only fluorescence emission from the

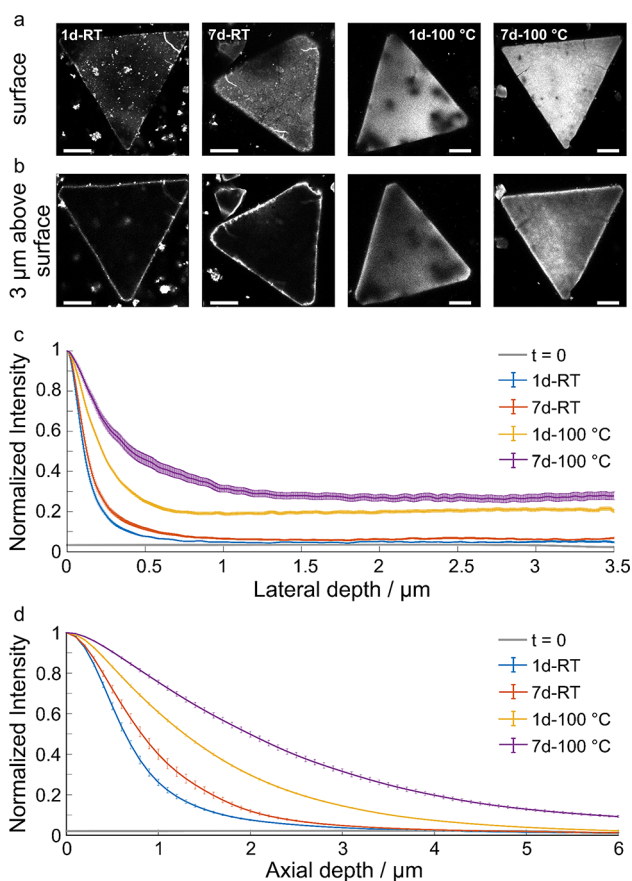


**Figure 3.** Fluorescence imaging of UiO-67 crystals after PSE in MeOH/DMF: (a) fluorescence images taken at the surface and (b) 3 μm above the surface. The scale bar is 15 μm. (c) Fluorescence intensity profile along lateral and (d) axial directions (error bars from measurements on 8–10 crystals of UiO-67 per condition). The curves recorded at  $t = 0$  (before any PSE takes place) display the autofluorescence of the pristine crystals (Figure S8).

crystal surface was observed (Figure S6), indicating that RB itself cannot diffuse through the window, let alone the bulkier BPDC-RB. Alternatively, through-backbone diffusion becomes a plausible mechanism to account for the slow penetration of BPDC-RB.

To elucidate the mechanism of linker migration, we employed FLIM, a technique used to acquire spatially resolved fluorescence lifetime information. In the phasor approach, the obtained fluorescence lifetime decay (Figure 4a) is transformed into Fourier space followed by a graphical translation into a phasor plot,<sup>24,25</sup> with long lifetimes near (0.5, 0.5) and short ones near (1, 0) (Figure 4b, section S1.6 in the Supporting Information). In a previous study, we established a correlation between the fluorescence lifetime and local defects in UiO-67: more defects result in shorter lifetime.<sup>26</sup> Thus, by using BPDC-RB as both a PSE participant and a fluorescence lifetime reporter, we investigated the formation and spatial distribution of defects accompanying the progression of PSE. The measured lifetime values vary from 0.65 ns (high defect level) to 2.91 ns (low defect level) (Figures S16–S20). A lifetime of 2.91 ns is even larger than the lifetime of BPDC-RB in solvents (2.1–2.3 ns) (Table S1), suggesting suppression of nonradiative pathways and stabilization of fluorescence in the MOF.

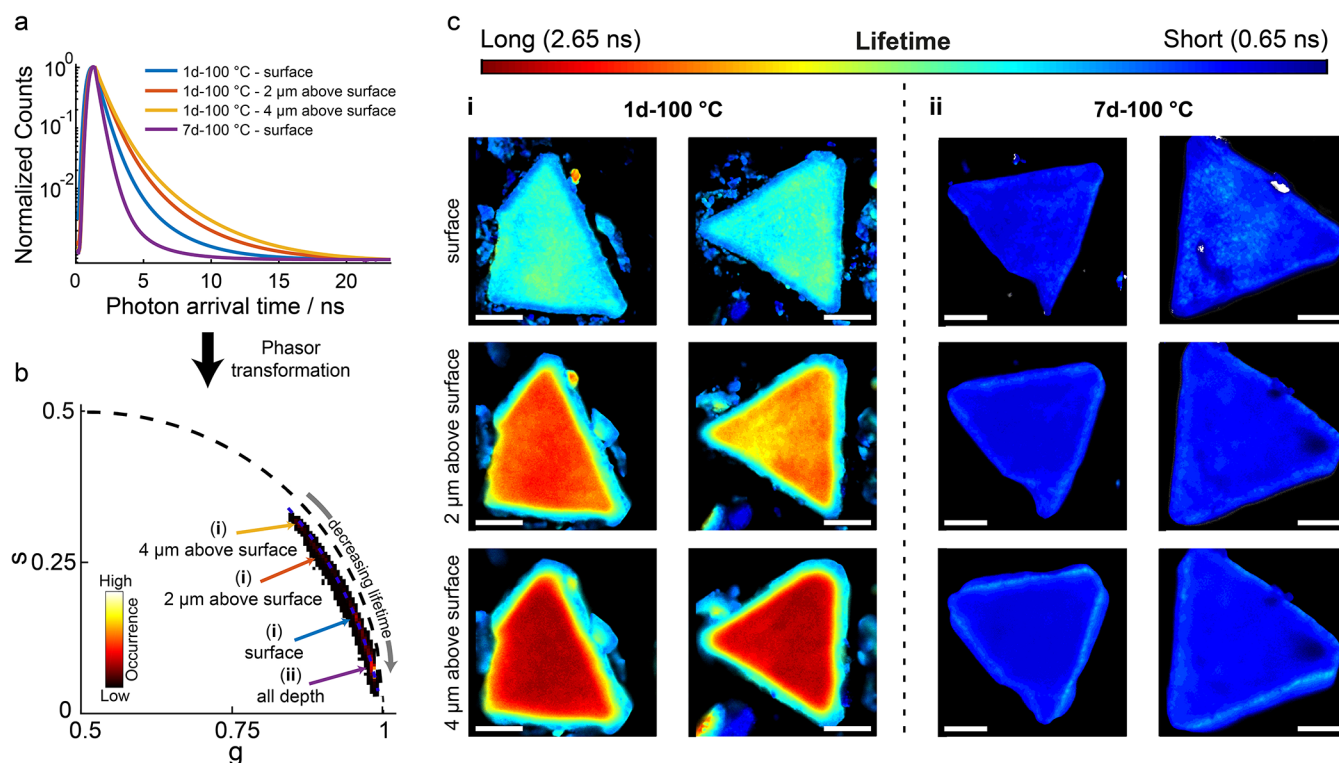


**Figure 4.** Fluorescence lifetime analysis of UiO-67 crystals after PSE in MeOH/DMF: (a) fluorescence lifetime decay, (b) phasor plot of lifetime, and (c) FLIM images of UiO-67 crystals. The scale bar is 15  $\mu\text{m}$ .

For PSE conducted for 1 day at 100  $^{\circ}\text{C}$ , the FLIM results displayed significant differences in lifetime between the crystal surface and interior (Figure 4c(i)). The lifetimes measured at the surface ( $1.36 \pm 0.22$  ns) are shorter than those inside the crystals. The FLIM images taken at 2  $\mu\text{m}$  above surface showed a lifetime of  $2.14 \pm 0.20$  ns at the core while the edge exhibited the same short lifetime observed for the surface plane. By shifting the focal plane deeper (4  $\mu\text{m}$  above surface), even longer lifetimes ( $2.55 \pm 0.15$  ns) were observed in the crystal core, establishing a gradient of lifetime increasing from the edge to the center. Interestingly, such a gradient in lifetime is analogous to the previously measured fluorescence profile, which exhibits a decay in fluorescence intensity from the outside toward inside of the crystal. This correlation suggests that the progression of PSE is accompanied by the generation of missing-linker defects, i.e., PSE leaves defects in its wake.

There are two possible origins for the missing-linker defects. The first possibility is that MeOH, a PSE solvent, can replace the original BPDC linker in UiO-67 by coordinating to the zirconium clusters. However, this process alone cannot establish and maintain a defect gradient more than 1 day, because the diffusion of methanol is largely unimpeded due to its small size. This claim is supported by previous observations that the incorporation of linker-substituting MeOH into UiO-67 plateaued within 1 day, even at 40  $^{\circ}\text{C}$ .<sup>18</sup> An alternative explanation for the observed gradient of missing-linker defects would be that these defects are the product of PSE according to the through-backbone diffusion mechanism. This mechanism agrees well with our observation that there are more defects on the surface where many through-backbone trajectories start from and fewer defects in the core where only a few PSE events reach this depth.

Prolonged PSE for 7 days at 100  $^{\circ}\text{C}$  resulted in a higher level of fluorescence quenching; a shorter lifetime of  $0.90 \pm 0.21$  ns was found. Interestingly, a homogeneous distribution of short lifetime was observed both at the surface and deeply in the interior of the crystals (Figure 4c(ii)). This is in contrast to the lifetime gradient observed for 1d-100  $^{\circ}\text{C}$  and matches the trend of PSE progression: the BPDC-RB concentration increases throughout the whole crystal when PSE is prolonged to 7 days (Figure 3c,d). Nevertheless, compared with the interior, the surface still has a higher level of PSE, but its defect level does not increase correspondingly. This might result from an equilibrium between defect generation and healing at high levels of PSE; replaced BPDC linkers can be reincorporated and thus heal missing-linker defects during their migration toward the outside, the opposite direction of BPDC-RB migration. This hypothesis is supported by a careful investigation of the FLIM data, which exhibits slightly higher lifetime at the surfaces compared to the interior (Figure S20).

We further investigated PSE at RT and found long lifetimes (Figures S16–S18) and hence low concentrations of defects, consistent with the low level of BPDC-RB incorporation. Extension of PSE from 1 day to 7 days led to a moderate decrease in lifetime. Likewise, PSE conducted in pure DMF resulted in a similar yet less pronounced temperature dependence: higher fluorescence lifetimes were observed at RT as compared to 100  $^{\circ}\text{C}$ , the latter showing a lifetime gradient from outside toward inside (Figures S21–S25). We argue that PSE at RT is in general unproductive because it failed to initiate the dissociation of BPDC, an energetically expensive step yet a prerequisite for the subsequent through-backbone diffusion of BPDC-RB. Once this energy barrier is overcome and the migration of BPDC-RB is initiated, more and more missing-linker defects will be created. These defects

can act to accelerate the following PSE events by opening the narrow windows, making the whole process autocatalytic. This highlights the importance of finding the optimal conditions for performing PSE with bulky linkers.

Our studies of PSE using BPDC-RB present a unique scenario where only through-backbone diffusion is possible. For linkers smaller than the MOF window, we envision that both through-backbone diffusion and through-window diffusion can occur. PSE will proceed via the mechanism that is most efficient. We expect that PSE via through-backbone diffusion is applicable to many other MOFs, allowing for the incorporation of sizable, sophisticated functional groups.

## ■ ASSOCIATED CONTENT

### SI Supporting Information

The Supporting Information is available free of charge at <https://pubs.acs.org/doi/10.1021/jacs.1c04804>.

Experimental, crystallographic, photophysical, and microscopy data including PXRD, SEM, fluorescence spectroscopy, and FLIM results (PDF)

## ■ AUTHOR INFORMATION

### Corresponding Authors

**Zhe Ji** – Department of Chemistry, University of California-Berkeley, Berkeley, California 94720, United States; Present Address: Department of Chemistry, Stanford University, Stanford, CA 94305; [orcid.org/0000-0002-8532-333X](https://orcid.org/0000-0002-8532-333X); Email: [zheji@stanford.edu](mailto:zheji@stanford.edu)

**Stefan Wuttke** – Department of Chemistry and Center for NanoScience, University of Munich, 81377 Munich, Germany; BCMaterials (Basque Center for Materials, Applications & Nanostructures), 48940 Leioa, Spain; IKERBASQUE, Basque Foundation for Science, 48009 Bilbao, Spain; [orcid.org/0000-0002-6344-5782](https://orcid.org/0000-0002-6344-5782); Email: [stefan.wuttke@bcmaterials.net](mailto:stefan.wuttke@bcmaterials.net)

### Authors

**Nader Al Danaf** – Department of Chemistry and Center for NanoScience, University of Munich, 81377 Munich, Germany

**Waldemar Schrimpf** – Department of Chemistry and Center for NanoScience, University of Munich, 81377 Munich, Germany

**Patrick Hirschle** – Department of Chemistry and Center for NanoScience, University of Munich, 81377 Munich, Germany

**Don C. Lamb** – Department of Chemistry and Center for NanoScience, University of Munich, 81377 Munich, Germany; [orcid.org/0000-0002-0232-1903](https://orcid.org/0000-0002-0232-1903)

Complete contact information is available at: <https://pubs.acs.org/doi/10.1021/jacs.1c04804>

### Notes

The authors declare no competing financial interest.

## ■ ACKNOWLEDGMENTS

We thank O. M. Yaghi (University of California, Berkeley) for providing resources, mentorship, support, and helpful discussions. We thank H. Wang (University of California, Berkeley) for help with the NMR data analysis. We are grateful for financial support from the Deutsche Forschungsgemeinschaft (DFG) and the SFB1032 (Project-B3, D.C.L.). We also thankfully acknowledge the support of the Excellence Cluster Nanosystems Initiative Munich (NIM), the Center for

NanoScience Munich (CeNS), and the LMU innovative BioImaging Network.

## ■ REFERENCES

- (1) Furukawa, H.; Cordova, K. E.; O’Keeffe, M.; Yaghi, O. M. The Chemistry and Applications of Metal–Organic Frameworks. *Science* **2013**, *341* (6149), 1230444.
- (2) Eddaoudi, M.; Kim, J.; Rosi, N.; Vodak, D.; Wachter, J.; O’Keeffe, M.; Yaghi, O. M. Systematic Design of Pore Size and Functionality in Isoreticular MOFs and Their Application in Methane Storage. *Science* **2002**, *295* (5554), 469–472.
- (3) Ji, Z.; Wang, H.; Canossa, S.; Wuttke, S.; Yaghi, O. M. Pore Chemistry of Metal–Organic Frameworks. *Adv. Funct. Mater.* **2020**, *30* (41), 2000238.
- (4) Cohen, S. M. The Postsynthetic Renaissance in Porous Solids. *J. Am. Chem. Soc.* **2017**, *139* (8), 2855–2863.
- (5) Cohen, S. M. Postsynthetic Methods for the Functionalization of Metal–Organic Frameworks. *Chem. Rev.* **2012**, *112* (2), 970–1000.
- (6) Haneda, T.; Kawano, M.; Kawamichi, T.; Fujita, M. Direct Observation of the Labile Imine Formation through Single-Crystal-to-Single-Crystal Reactions in the Pores of a Porous Coordination Network. *J. Am. Chem. Soc.* **2008**, *130* (5), 1578–1579.
- (7) Wang, Z.; Cohen, S. M. Postsynthetic Covalent Modification of a Neutral Metal–Organic Framework. *J. Am. Chem. Soc.* **2007**, *129* (41), 12368–12369.
- (8) Wu, C.-D.; Hu, A.; Zhang, L.; Lin, W. A Homochiral Porous Metal–Organic Framework for Highly Enantioselective Heterogeneous Asymmetric Catalysis. *J. Am. Chem. Soc.* **2005**, *127* (25), 8940–8941.
- (9) Seo, J. S.; Whang, D.; Lee, H.; Jun, S. I.; Oh, J.; Jeon, Y. J.; Kim, K. A homochiral metal–organic porous material for enantioselective separation and catalysis. *Nature* **2000**, *404* (6781), 982–986.
- (10) Kiang, Y. H.; Gardner, G. B.; Lee, S.; Xu, Z.; Lobkovsky, E. B. Variable Pore Size, Variable Chemical Functionality, and an Example of Reactivity within Porous Phenylacetylene Silver Salts. *J. Am. Chem. Soc.* **1999**, *121* (36), 8204–8215.
- (11) Kim, M.; Cahill, J. F.; Fei, H.; Prather, K. A.; Cohen, S. M. Postsynthetic Ligand and Cation Exchange in Robust Metal–Organic Frameworks. *J. Am. Chem. Soc.* **2012**, *134* (43), 18082–18088.
- (12) Deria, P.; Mondloch, J. E.; Karagiari, O.; Bury, W.; Hupp, J. T.; Farha, O. K. Beyond post-synthesis modification: evolution of metal–organic frameworks via building block replacement. *Chem. Soc. Rev.* **2014**, *43* (16), 5896–5912.
- (13) Karagiari, O.; Lalonde, M. B.; Bury, W.; Sarjeant, A. A.; Farha, O. K.; Hupp, J. T. Opening ZIF-8: a catalytically active zeolitic imidazolate framework of sodalite topology with unsubstituted linkers. *J. Am. Chem. Soc.* **2012**, *134* (45), 18790–6.
- (14) Karagiari, O.; Bury, W.; Sarjeant, A. A.; Stern, C. L.; Farha, O. K.; Hupp, J. T. Synthesis and characterization of isostructural cadmium zeolitic imidazolate frameworks via solvent-assisted linker exchange. *Chemical Science* **2012**, *3* (11), 3256–3260.
- (15) Boissonault, J. A.; Wong-Foy, A. G.; Matzger, A. J. Core–Shell Structures Arise Naturally During Ligand Exchange in Metal–Organic Frameworks. *J. Am. Chem. Soc.* **2017**, *139* (42), 14841–14844.
- (16) Cavka, J. H.; Jakobsen, S.; Olsbye, U.; Guillou, N.; Lamberti, C.; Bordiga, S.; Lillerud, K. P. A New Zirconium Inorganic Building Brick Forming Metal Organic Frameworks with Exceptional Stability. *J. Am. Chem. Soc.* **2008**, *130* (42), 13850–13851.
- (17) Liu, Y.; Ma, Y.; Yang, J.; Diercks, C. S.; Tamura, N.; Jin, F.; Yaghi, O. M. Molecular Weaving of Covalent Organic Frameworks for Adaptive Guest Inclusion. *J. Am. Chem. Soc.* **2018**, *140* (47), 16015–16019.
- (18) Marreiros, J.; Caratelli, C.; Hajek, J.; Krajnc, A.; Fleury, G.; Bueken, B.; De Vos, D. E.; Mali, G.; Roeffaers, M. B. J.; Van Speybroeck, V.; Ameloot, R. Active Role of Methanol in Post-Synthetic Linker Exchange in the Metal–Organic Framework UiO-66. *Chem. Mater.* **2019**, *31* (4), 1359–1369.
- (19) Morabito, J. V.; Chou, L.-Y.; Li, Z.; Manna, C. M.; Petroff, C. A.; Kyada, R. J.; Palomba, J. M.; Byers, J. A.; Tsung, C.-K. Molecular

Encapsulation beyond the Aperture Size Limit through Dissociative Linker Exchange in Metal–Organic Framework Crystals. *J. Am. Chem. Soc.* **2014**, *136* (36), 12540–12543.

(20) Becker, W. Fluorescence lifetime imaging–techniques and applications. *J. Microsc.* **2012**, *247* (2), 119–36.

(21) Ameloot, R.; Vermoortele, F.; Hofkens, J.; De Schryver, F. C.; De Vos, D. E.; Roeyers, M. B. Three-dimensional visualization of defects formed during the synthesis of metal-organic frameworks: a fluorescence microscopy study. *Angew. Chem., Int. Ed.* **2013**, *52* (1), 401–5.

(22) Schrimpf, W.; Ossato, G.; Hirschle, P.; Wuttke, S.; Lamb, D. C. Investigation of the Co-Dependence of Morphology and Fluorescence Lifetime in a Metal-Organic Framework. *Small* **2016**, *12* (27), 3651–7.

(23) Connolly, B. M.; Aragoes-Anglada, M.; Gandara-Loe, J.; Danaf, N. A.; Lamb, D. C.; Mehta, J. P.; Vulpe, D.; Wuttke, S.; Silvestre-Albero, J.; Moghadam, P. Z.; Wheatley, A. E. H.; Fairen-Jimenez, D. Tuning porosity in macroscopic monolithic metal-organic frameworks for exceptional natural gas storage. *Nat. Commun.* **2019**, *10*, 2345.

(24) Digman, M. A.; Caiolfa, V. R.; Zama, M.; Gratton, E. The Phasor Approach to Fluorescence Lifetime Imaging Analysis. *Biophys. J.* **2008**, *94* (2), L14–L16.

(25) Redford, G. I.; Clegg, R. M. Polar Plot Representation for Frequency-Domain Analysis of Fluorescence Lifetimes. *J. Fluoresc.* **2005**, *15* (5), 805.

(26) Schrimpf, W.; Jiang, J.; Ji, Z.; Hirschle, P.; Lamb, D. C.; Yaghi, O. M.; Wuttke, S. Chemical diversity in a metal-organic framework revealed by fluorescence lifetime imaging. *Nat. Commun.* **2018**, *9*, 1647.